EXPERIMENTAL AND NUMERICAL INVESTIGATION OF A GEARLESS ONE-MOTOR CONTRA-ROTATING FAN

Martin HEINRICH[1], Christian FRIEBE[2],
Franziska BOTHE[1], Rüdiger SCHWARZE[1]

[1] *Technical University Bergakademie Freiberg, Institute of Mechanics and Fluid Dynamics, Lampadiusstraße 4, 09599 Freiberg,*

[2] *Institut für Luft- und Kältetechnik gGmbH (ILK), Bertolt-Brecht-Allee 20, 01309 Dresden, Germany*

SUMMARY

A gear-less one-motor concept for contra-rotating fans is presented in this paper. It was designed and experimentally investigated by the Institute of Air Handling and Refrigeration in Dresden. The performance map and 2D PIV measurements were conducted. The results are compared to 3D numerical computations using the k-omega SST turbulence model. The results show a good agreement for the performance map as well as velocity profiles.

NOMENCLATURE

Latin symbols

h	Hub-to-tip ratio
k	Turbulent kinetic energy
m	Mass
M	Momentum
n	Rotational speed
P	Shaft power
p	Pressure
$\dot{V}$	Flow rate

Greek symbols

λ	Coefficient of performance
ν	Kinematic viscosity
φ	Flow coefficient
ψ	Pressure rise coefficient
ω	Specific dissipation

Abbreviations

CRF	Contra-rotating fan
SRF	Single-rotor fan
SST	Shear-stress transport

INTRODUCTION

Compared to single rotor fans with discharge guide vanes, contra-rotating fans (CRF) reduce the swirl in the wake flow as well as achieve higher power densities. In practice, this approach is already being used to expand the application range of axial fans due to the higher total pressure rise and increased efficiency. Conventional contra-rotating fans utilize one motor for each rotor or a gear for power transmission. This installation is more complicated, expensive and requires more maintenance compared to single rotor fans.

In order to overcome these disadvantages, a new gearless one-motor concept was developed for compact fans at the Institute of Air Handling and Refrigeration in Dresden, Germany. Due to the innovative design, the torque is equally distributed between both rotors improving the flow field inside the fan. Further advantage is the reduced swirl in the wake flow which results in less energy losses and higher pressure and flow coefficients. The compact design makes the CRF favourable for various applications where large industrial fans cannot be used due to lack of space, e.g. tunnel and mine ventilation.

The system of CRF is known for many years. Already in the 1990s Sullivan *et al.* [1] performed tests with a true to scale model of a CRF in the wind tunnel from NASA and Boeing to determine the aerodynamic performances. Further experimental work was proceeded in [2-4] with the aim to reduce noise emission and fuel consumption. However, there has been a lack of publications regarding the numerical simulation of contra-rotating fans. Brailko *et al*. [5] investigated the influence of the tip vortex on the noise generation. Cho *et al.* [6] showed how to design rotor blades and Wang *et al.* [7] investigated different blade pitch angels to validate and improve recommendations for shaft power matching of CRFs.

In this paper, a new contra-rotating fan concept is presented using only one gearless motor. The setup is explained and the CRF is investigated using a test bench to measure the performance map. Furthermore, stero PIV measurements behind the second rotor are performed. Finally, numerical simulations were performed to analyse the flow field in detail and validate the computational model.

CONTRA-ROTATING FAN

The new concept for a contra-rotating fan utilizes only one shaft for the drive train of the two fan blades (see *Figure 1*). Both are coupled using the momentum equilibrium. The electric motor is not mounted to a fixed position. Its internal rotor is connected to the first fan and the external rotor is connected to the second one. Therefore, if the electric motor starts spinning, the first fan as well as the second one start turning. For this reason, a contactless power transmission is needed to supply power to the motor. Due to the law of conservation of angular momentum, the magnitude of the momentum of both fans is always equal

$$M_1 = -M_2 \tag{1}$$

with the power of each rotor defined as

$$P_\mathrm{i} = 2\pi M_\mathrm{i} n_\mathrm{i} \tag{2}$$

with

$$P = P_1 + P_2 \tag{3}$$

and

$$\frac{n_1}{|n_1|} = 1 \quad , \quad \frac{n_2}{|n_2|} = -1 \ . \tag{4}$$

The characteristics for the first and second fan rotor are shown in *Table 1*. The first one was manufactured by ebm-pabst and consists of 9 blades made of steel sheet. The design speed is at 2100 min^{-1} with a maximum static pressure rise of 100 Pa. The design of the second rotor is based on the analytic velocity profiles of the first fan. It has 11 single blades made by selective-laser-sintering using polyamide PA2200 and are mounted on an aluminum ring. The hub has a total length of 290 mm and an inner diameter of 90 mm. Three struts are used at the spinner as well as behind second rotor to connect the fan with the housing.

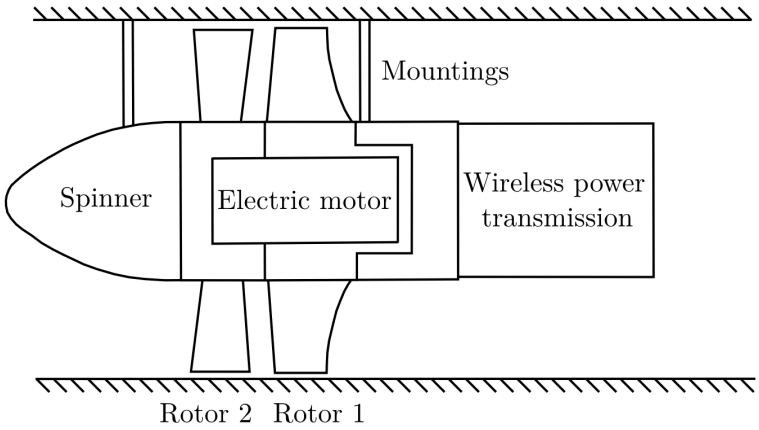

Figure 1: Basic setup of the contra-rotating fan.

Table 1: Characteristics of the first and second rotor.

		Rotor 1	Rotor 2
Max. static pressure rise	Δp_{max}	100 Pa	40 Pa
Rotational speed	n	2100 min^{-1}	1200 min^{-1}
Shroud diameter	D	0,2 m	0,2 m
Hub-to-tip ratio	h	0,45	0,45
Mass	m	2,13 kg	0,45 kg
Material	-	Steel sheet	Polyamide PA2200 with aluminum hub

EXPERIMENTAL SETUP

The measurements were performed on a test rig based on DIN EN ISO 5801:2011 (see *Figure 2*). It has a total length of 2.4 m and a pipe diameter of 200 mm. It consists of three parts: (1) the air inflow channel with a curved inlet nozzle, (2) the fan and (3) the outlet with a flow control value to adjust the flow rate. The inlet nozzle is used to achieve a homogeneous velocity profile and measure the mass flow rate using four pressure tabs at the tube walls. Four pressure tabs at the outlet pipe are used for the calculation of the static pressure rise of the fan. The shroud of the fan is made of acrylic glass to enable optical access for PIV measurements.

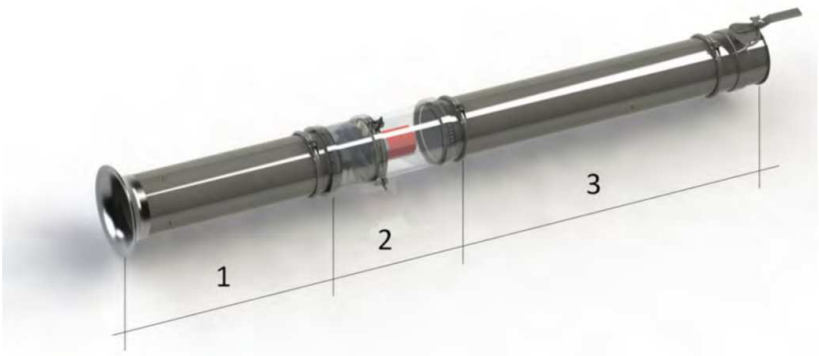

Figure 2: Test rig with (1) air inflow channel, (2) fan and (3) outlet with flow control.

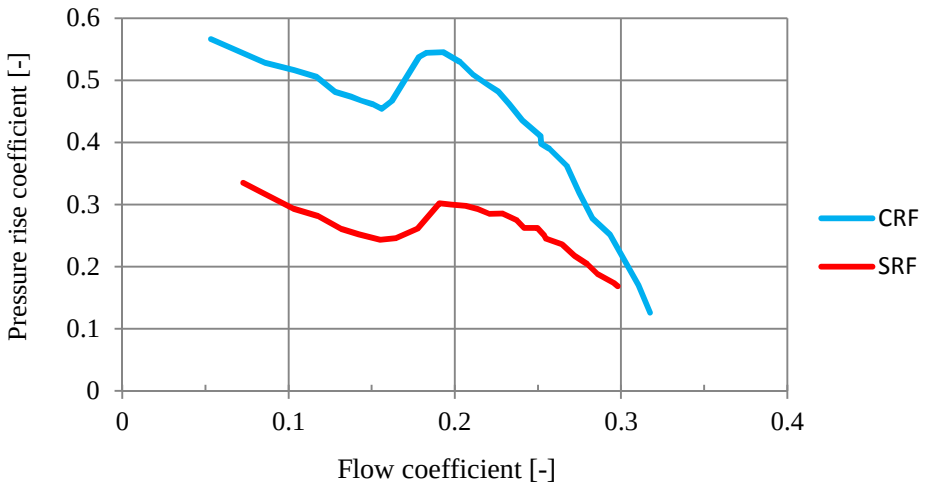

Figure 3: Measured performance map for the single-rotor fan (SRF) and the contra-rotating fan (CRF).

EXPERIMENTAL RESULTS

The experimental measurements were conducted by Czarnecki [8] at the ILK. Two of them were chosen for this publication. The first one is a standard single-rotor fan (SRF) using the first rotor only. In this case, the second rotor is replaced by a straight pipe. The other aspects of the setup are the same as for the CRF. In the second case, the contra-rotating fan is analyzed. The flow and pressure rise coefficients as well as the coefficient of performance are defined as follows

$$\varphi = \frac{\dot{V}}{\frac{\pi^2}{4} D^3 n_1}, \quad \psi = \frac{\Delta p}{\frac{\pi^2}{2} D^2 n_1^2 \rho}, \quad \lambda = \frac{P_F}{\frac{\pi^4}{8} D^5 n_1^3 \rho} \tag{3}$$

The experimental measurements of the fan performance can be seen in *Figure 3*. The pressure rise of the contra-rotating fan is considerably higher compared to the single-rotor fan. The reason for this is the second rotor, which reduces the swirl in the wake of the fan and therefore increases the static pressure rise. However, the shapes of the performance curves are very similar and the maxima are nearly at the same flow rate. The coefficient of performance is shown in *Figure 4*. As expected, the power density of the CRF is significantly higher than the one of the SRF. Furthermore, the maximum performance is shifted slightly to lower flow rates.

Figure 5 shows the different angular velocities of the first and second rotor for the CRF. These vary by up to 20% with respect to the design speed. For that reason, the design speed cannot be used for

the numerical simulations. The actual rotational speed, which is different for each operating point, has to be adjusted according to the experiments.

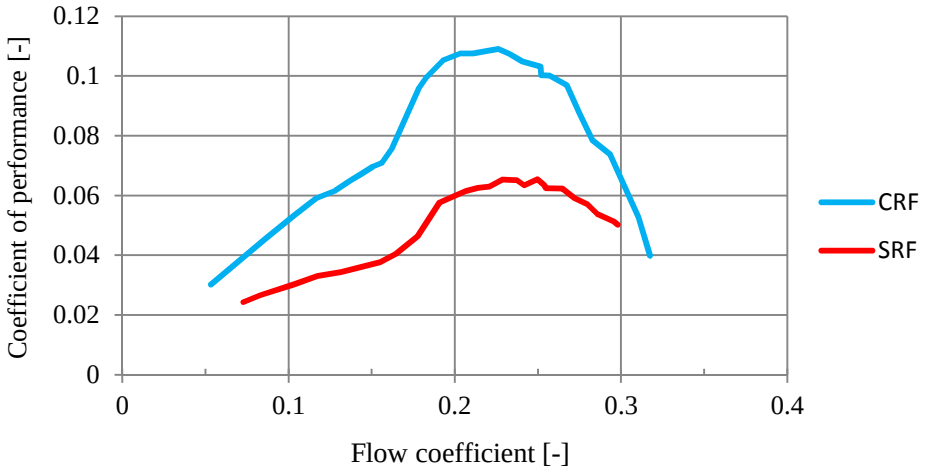

Figure 4: Measured coefficient of performance for the single-rotor (SRF) and contra-rotating fan (CRF).

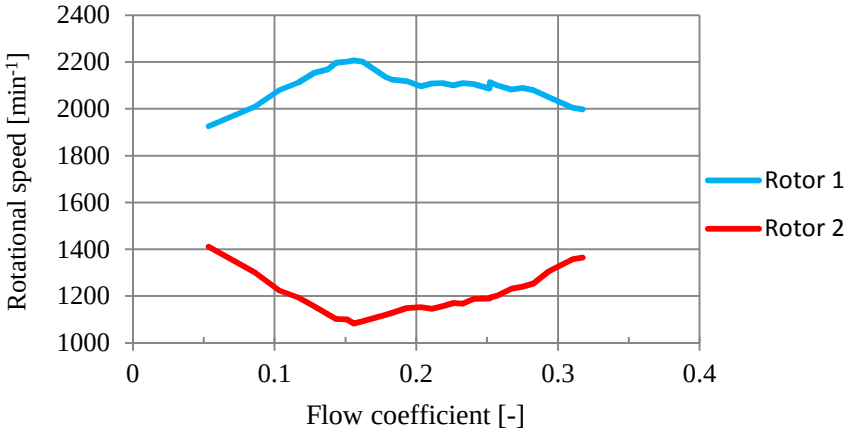

Figure 5: Rotational speed of the first and second fan for the contra-rotating fan.

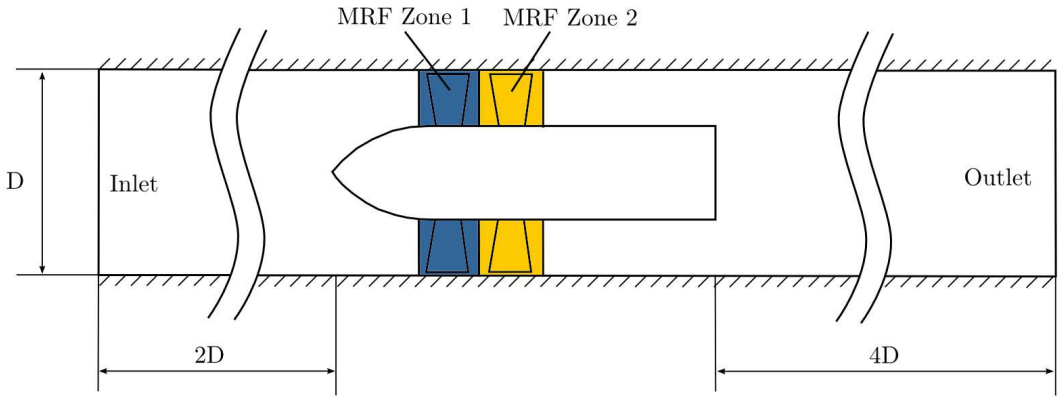

Figure 6: Numerical Model

NUMERICAL SETUP

A numerical model of the test bench was created (see *Figure 6*). It consists of the air inflow channel, the contra-rotating fan and the outlet channel. The rotation of the fans is modelled using the Multiple-Reference-Frame (MRF) approach. The mesh is fixed in space and additional terms are added to the momentum equation to account for the rotation. The mesh is refined in the wake of the blades is used. Furthermore, mesh extrusion has been used for the inlet and outlet channel, where the inlet pipe is twice the diameter and the outlet pipe four times the diameter long. This reduces the boundary effects onto the numerical solution. Five different mesh sizes (4.02 – 10.30 x 10^6 cells) were used to assess the mesh influence (see *Figure 7*). The mesh with about 5.66 x 10^6 cells shows the best compromise between accuracy and computational cost.

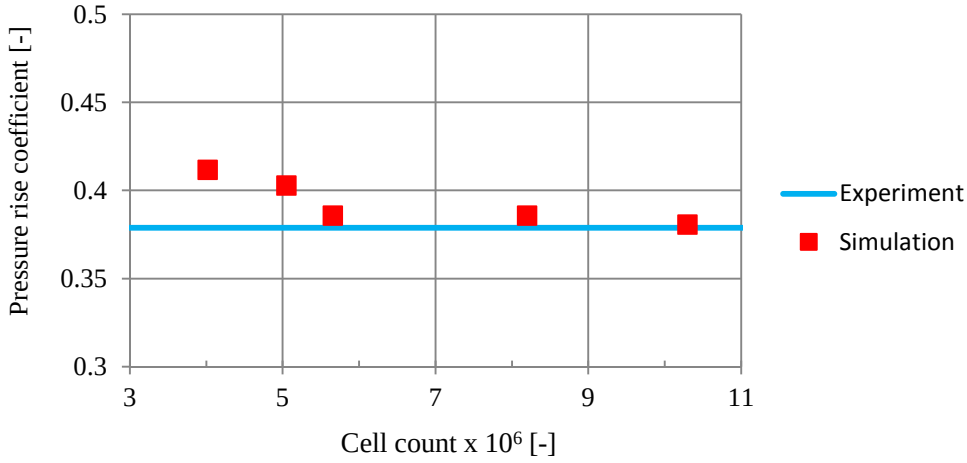

Figure 7: Pressure rise coefficient at design point as a function of the cell count.

At the inlet, a fully developed profile for the velocity and the turbulent quantities is specified. The average inlet velocity is modified to realize different flow coefficients. At the outlet, the relative static pressure with respect to the ambient conditions is set to 0 Pa and the other variables are treated as zero gradient. The fluid is air with a kinematic viscosity of $\nu = 1.85 \cdot 10^{-5} \mathrm{m}^2/\mathrm{s}$.

The open-source CFD library OpenFOAM Version 2.3.x [9] is used for the simulation. A incompressible steady-state solver is chosen based on the SIMPLE algorithm. The k-omega SST turbulence model [10] is employed with wall functions. The discretization is second order upwind for the momentum and first order for the turbulent quantities. The final residuals are set to 10^{-5}. Furthermore, the static pressure at the inlet is monitored to judge convergence.

Figure 8 shows the performance map of the contra-rotating fan for the simulation and experiment. At higher flow rates, the accordance is good. The slope is slightly underpredicted, though. At lower velocities, the magnitude of the maximum pressure coefficient is reached. However, the simulation predicts it at a lower flow rate. In general, the instable region of the performance map is not predicted accurately. One reason for this might be the steady-state MRF-approach, which does not account for the unsteady behavior of the flow. Furthermore, rotor-rotor interactions are greatly simplified. The coefficient of performance of the experiment and the simulation is shown in Figure ***9***. The differences between the numerical model and the experiment are less than 5% and the slopes are met well. However, the maximum value of 0.107 is slightly overpredicted to higher flow rates.

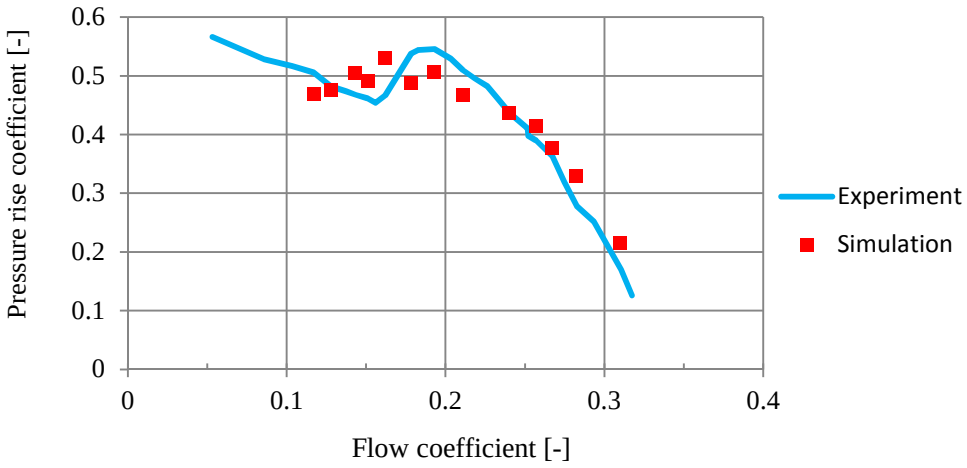

Figure 8: Comparison of numerical and experimental results for the contra-rotating fan.

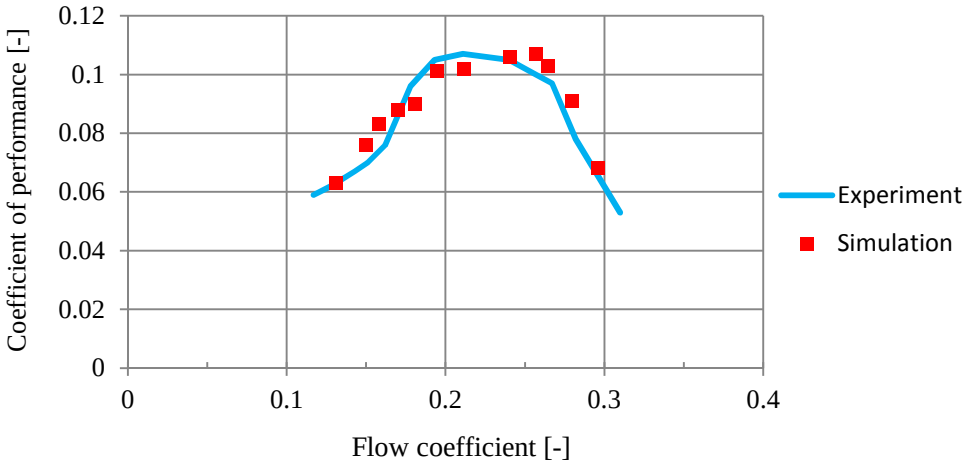

Figure 9: Coefficient of performance for the experiment and the simulation.

Stereo-PIV measurements were performed to acquire detailed velocity fields behind the second rotor. Figure 10 shows the circumferential averaged axial flow velocity for the simulations and the experiment 30 mm behind the second rotor. The velocity profile is met very well by the numeric model and the radial position of the maximum is predicted correctly. However, the maximum axial velocity is slightly overestimated.

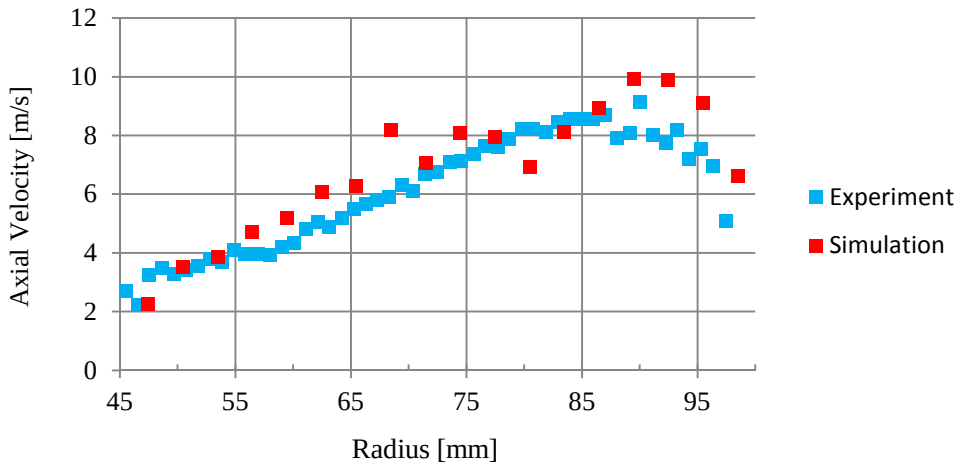

Figure 10: Circumferential averaged axial velocity of the simulation and experiment 30 mm behind the second rotor.

CONCLUSION

A gear-less one-motor concept for contra-rotating fans was presented in this paper. For comparison, the single-rotor and the contra-rotating fan were experimentally investigated and the performance curve for the design speed of 2100 rpm was measured. As expected, the CRF showed a significantly higher pressure coefficient and coefficient of performance. Furthermore, a numerical model was developed for the CRF and validated using the measurement data. The results show, that the simulation is capable of resolving the flow field of the fan and accurately predict the performance curve as well as local velocity profiles.

BIBLIOGRAPHY

[1] P.B. Sullivan, Y.O. Jain, D.S. Pundhir – *Aerodynamic performance of a scale-model, counter-rotating unducted fan*. Journal of Turbomachinery, **112**(4), pp. 579-586, **1990**

[2] H.-W. Shin, C.E. Whitfield, D.C. Wisler – *Rotor-rotor interaction for counter-rotating fans, part1: Three-dimensional flowfield measrements*, AIAA Journal, **32**(11), pp. 2224-2233, **1994**

[3] Q. Li, Z. Li, Y. Lu – *Experimental study on the unsteady flow between rotors of counter-rotating fan*. Progress in Natural Science, **12**(4), pp. 289-293, **2002**

[4] Z.J. Ai, L. Wu, F.W. Jin – *Research on performance testing and analysis system about counter-rotating fan based on labview*. Advanced Materials Research, **467-471**, pp. 1426-1430, **2012**

[5] I.A. Brailko, V.I. Mileshin, M.A. Nyukhtikov, S.V. Pankov – *Computational and experimental investigation of unsteady and acoustic characteristics of counter-rotating fans*. ASME 2004 Heat Transfer/Fluids Engineering Summer Conference, Vol. 2, pp. 871-879, **2004**

[6] L. Cho, H. Choi, S. Lee, J. Cho – *Numerical and experimental analysis for the aerodynamic design of high performance counter-rotating axial flow fans.* ASME 2009 Fluids Engineering Division Summer Conference, Vol. 2, pp. 231-244, **2009**

[7] W. Wang, S. Li, Z. Zhu, D. Huang, K. Zhu – *Shaft power matching and performance preduction for contra-rotating axial flow fans.* HVAC&R Research, **13**(1), pp. 141-162, **2007**

[8] T. Czarnecki – *Aufbau und Messung eines gegenläufigen Axial-Kompaktlüfters*. Bachelorarbeit RWTH Aachen University, E.ON Energieforschungszentrum. Lehrstuhl für Gebäude- und Raumklimatechnik. **2014**

[9] OpenFOAM, Version 2.3.x – `http://www.openfoam.com` **2014**

[10] F. Menter – *Two-Equation Eddy-Viscosity Turbulence Models for Engineering Applications.* AIAA Journal, Vol. 32, pp. 1598-1605. **2014**